

DEVELOPMENT OF A LOW COST AND SAFE PIV FOR MEAN FLOW VELOCITY AND REYNOLDS STRESS MEASUREMENTS

Mohammad Rostami*, Abdullah Ardeshir

Department of Civil and Environmental Engineering, Amirkabir University of Technology
Tehran, Iran, m_rostami@aut.ac.ir

Goodarz Ahmadi

Department of Mechanical and Aeronautical Engineering, Clarkson University
Potsdam, NY, USA, ahmadi@clarkson.edu

Peter Joerg Thomas

Department of Engineering, University of Warwick
Coventry, UK, eddy.decay@eng.warwick.ac.uk

*Corresponding Author

(Received: May 31, 2006 – Accepted in Revised Form: May 31, 2007)

Abstract In this study, a white light particle image velocimetry (WL PIV) system which employs a light sheet generated with a flash was used. The system was developed in order to provide a cost-efficient and safe alternative to laser systems while keeping the accuracy limits required for hydraulic model tests. To investigate the accuracy of WL PIV method under different flow conditions, experiments were done at three different values of flow rates. Then the velocity vectors of each flow rate through the flume were calculated by means of cross-correlation of the two subsequent images. Flow velocity and Reynolds stress of each experiment were measured. The accuracy and integrity of the experiments were validated by comparison to the results which were obtained with empirical models of the mean velocity and Reynolds stress distribution in the boundary layer. Excellent agreement between the experimental and empirical results was observed. The whole flow field from the entrance of the experimental flume to its outlet was also modeled computationally using the Reynolds averaged Navier-Stokes equations and the k- ϵ turbulence model of FLUENTTM code. It was found that the WL PIV measurements had a deviation of about 0.5 to 1.5% from the computational results which provides further evidence that WL PIV can be applied successfully in open channel flow analysis.

Keywords Flow Velocity, WL PIV, Reynolds Stress, Empirical Models, FLUENTTM Code

چکیده در این تحقیق، از یک منبع نور سفید PIV برای ایجاد یک صفحه نور در امتداد جریان استفاده شده است. توسعه این سیستم اندازه‌گیری ضمن اینکه دقت مورد نظر مدل‌های هیدرولیکی را تامین می‌کند، در مقایسه با سیستم لیزری، گزینه‌ای مطمئن و کم هزینه است. برای بررسی دقت این روش، آزمایش‌هایی با سه بده جریان انجام شد. سپس میدان سرعت هریک از بده‌ها با استفاده از همبستگی عرضی تصاویر تهیه شده توسط یک دوربین سرعت بالا، بدست آمد. سرعت جریان و تنش رینولدز برای هر یک از آزمایش‌ها اندازه‌گیری شد. دقت و صحت نتایج داده‌های آزمایشگاهی در مقایسه با نتایج روابط تجربی توزیع متوسط سرعت و تنش رینولدز در لایه مرزی بررسی شد. انطباق بسیار خوبی بین نتایج آزمایشگاهی و تجربی مشاهده گردید. میدان جریان نیز توسط نرم افزار FLUENTTM به صورت عددی و با استفاده از معادلات ناویر-استوکس و مدل آشفتگی k- ϵ مدلسازی شد و دقت و صحت نتایج آزمایشگاهی به روش PIV در مقایسه با نتایج عددی ارزیابی گردید. نتایج نشان داد که اختلاف بین داده‌های آزمایش PIV نور سفید و نتایج عددی برای سه بده مورد آزمایش در حدود ۰/۵ تا ۱/۵ درصد است که حاکی از امکان استفاده مطمئن این روش برای تحلیل جریان کانال روباز می‌باشد.

1. INTRODUCTION

As is well acknowledged, physical variables to

describe fluid motion are functions of space and time. Therefore, experimentalists in fluid mechanics have been seeking measuring methods

to obtain spatio-temporal information about the flow field. One of the important physical variables can describe the fluid flow is the velocity profile. Numerous techniques have been established for measuring the flow velocity profile in physics and engineering. These techniques measure the unsteady flow fluctuations of pressure and velocity at single points on surfaces (pressure transducers, hot-film etc.) or single points in the flow field (LDA, L2F, hotwire probes etc.) [1]. However, all of these methods have one thing in common which is that they cannot resolve the instantaneous features of the flow field, but can only provide field velocity data in statistical form [2]. In contrast to these traditional single-point velocity measurement techniques, Particle Image Velocimetry (PIV) is able to provide instantaneous flow field data [3-5]. The PIV is a quantitative velocity measurement technique, which visualizes the flow field by small tracer particles and by analyzing the visualized digital images [6]. This technique can measure the whole two-dimensional or three-dimensional flow field simultaneously without disturbing the flow field [7]. The PIV has a large range of applications, from slow flows modeled in a laboratory environment to transonic and supersonic flows produced in industrial wind tunnels and turbine engines [8-10].

It should be noted that the focus of the present paper is on comparison of data obtained through a PIV system and those obtained with both empirical models and numerical simulation (CFD) in a representative flow of practical interest in hydraulic engineering. To measure the velocity of the fluid, the flow was seeded with small tracer particles that follow the fluid faithfully. A plane of the flow was illuminated by a thin sheet of light. In the present study, a white light PIV system was developed in order to provide a cost-effective and safe alternative for laser systems while keeping the accuracy limits required for hydraulic model tests. The images of the tracer particles within the plane were recorded twice with a very small time delay of Δt onto a high-speed camera. Then the velocity vectors of flow through the experimental flume were calculated by means of cross-correlation of the two subsequent images. The mean velocity and Reynolds stress distribution in a test section were examined in comparison with empirical results. In

the following, to find the accuracy of the PIV results, the flow was also modeled computationally using the two-dimensional Reynolds-averaged Navier-Stokes equations and the k- ϵ turbulence model of FLUENTTM code.

2. PRINCIPLES OF PARTICLE IMAGE VELOCIMETRY

A typical configuration of a digital PIV system is shown in Figure 1. To measure the velocity of the fluid, the flow is seeded with small tracer particles that follow the fluid faithfully. A “plane” of the flow is illuminated by a thin sheet of light, usually laser light, and the images of the tracer particles within the “plane” are recorded twice with a very small time delay of Δt onto either a film (photographic or holographic) or a CCD (charge-coupled device) array. The usual method for the evaluation of two images separated by a small finite time step is called cross-correlation. The cross-correlation function for two discretely sampled images is defined as:

$$R_{fg}(m,n) = \sum_i \sum_j f(i,j) \times g(i+m,j+n) \quad (1)$$

with $f(i,j)$ and $g(i,j)$ denoting the image intensity distribution of the first and second images, m and n , the pixel offset between the two images and $R_{fg}(m,n)$ the cross-correlation function. According to Figure 1, the digital image of the flow field is then subdivided into interrogation areas (IA) of 16×16 , 32×32 or 64×64 pixel size. The interrogation areas from each image frame, I1 and I2, are cross-correlated with each other, pixel by pixel. A displacement vector map over the whole target area is obtained by repeating the cross-correlation for each interrogation area over the two image frames captured by the camera. The correlation of the two interrogation areas, I1 and I2, results in the particle displacement ΔX , represented by a signal peak in the correlation $C(\Delta X)$.

The velocity vectors can then be analyzed by the displacement of the tracer particle images over the time between the exposure of the first frame and the second as follows [11]:

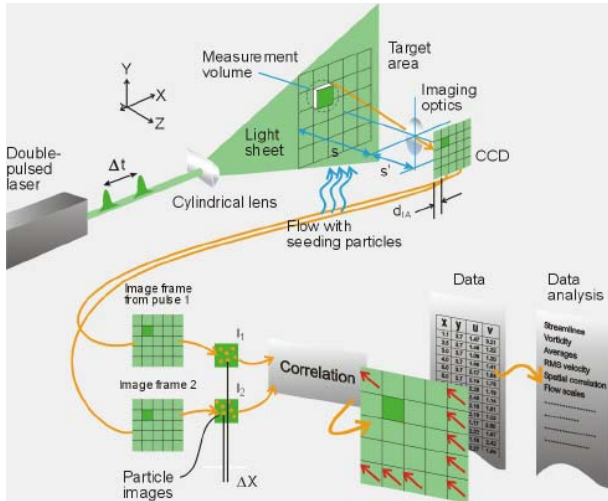


Figure 1. Experimental principle and general arrangement for PIV [11].

$$\bar{V} = \frac{\Delta \bar{X}}{\Delta t} \quad (2)$$

3. MEAN VELOCITY DISTRIBUTION OF THE TURBULENT FLOW

Although multiequation turbulence models are needed to predict velocity profiles in complex turbulent, Prandtl's mixing-length model remains valuable for the theoretical study of near-wall velocity profiles. For 2D uniform open-channel flow, four theoretical curves are given by [12,13]:

$$\frac{U}{U_\tau} = \frac{U_\tau y}{\nu} \quad \text{or} \quad U^+ = y^+ \quad \text{for} \quad \frac{U_\tau y}{\nu} \leq 5 \quad (3)$$

$$\frac{dU^+}{dy^+} = \frac{2(1-y^+/Re_\tau)}{1 + \sqrt{1 + 4\ell^{+2}(1-y^+/Re_\tau)}} \quad (4)$$

$$\text{for} \quad 5 \leq \frac{U_\tau y}{\nu} \leq 30$$

$$\frac{U}{U_\tau} = \frac{1}{k} \ln \frac{U_\tau y}{\nu} + A \quad (5)$$

$$\text{for} \quad 30 \leq \frac{U_\tau y}{\nu} \leq 0.2 Re_\tau \quad \text{and} \quad \frac{y}{\delta} < 0.2$$

$$\frac{U_{\max} - U}{U_\tau} = \frac{1}{k} \ln \left(\frac{y}{\delta} \right) \quad (6)$$

$$\text{for} \quad \frac{y}{\delta} > 0.2$$

Where U = flow velocity; Re_τ = Reynolds number based on the shear velocity U_τ and the hydraulic radius R ; δ = boundary layer thickness; A = integration constant. Nezu and Nakagawa [13] reviewed previous existing experimental data of k and A in steady wall shear flows with nearly zero-pressure gradient and concluded that the von Karman constant is universal, i.e., $k = 0.41$, independent of main flow properties such as open channels, pipe and boundary layers, whereas the integration constant A is not universal but dependent on flow properties and wall roughness {in general, $A = 5.0-5.5$ (smooth wall) and specially $A = 5.3$ in smooth open channels [14]}.

Equation 2 is theoretical formula in the viscous sublayer of $y^+ \leq 5$, Equation 4 is the log-law that is satisfied in the inner-wall region and Equation 5 is the outer region equation which is called the "velocity defect law" or "outer law". No analytical solution is available in the buffer layer of $5 \leq U_\tau y/\nu \leq 30$, but a numerical curve is obtained from Equation 3 which can be solved once ℓ^+ is specified. Prandtl proposed the well-known relation, $\ell^+ = ky^+$, where k is termed the von Karman constant. Very near the wall, viscous effects are not negligible, and must be reflected in the specification of ℓ^+ . The modified mixing-length model of van Driest [15] incorporates viscous effects as follows:

$$\ell^+ = ky^+ \Gamma \quad \text{and} \quad \Gamma = 1 - \exp(-y^+/26) \quad (7)$$

where Γ is termed the van Driest damping function.

4. NUMERICAL SIMULATION

It should be note that CFD codes are usually validated by comparing them to experimental results of high accuracy. But sometimes the experimental results can be validated by

comparison to well developed CFD results in which one has a high degree of confidence. Then, if the experimental results are in good agreement with the CFD results, the experimental results for other cases can be used for validation of CFD codes. Whereas the FLUENT CFD code has been utilized extensively to carry out a huge range of hydrodynamic flow simulations.

For an incompressible fluid flow, the equation of continuity and balance of momentum for the mean motion are given as [16]:

$$\frac{\partial}{\partial x_i}(\rho U_i) = 0 \quad (8)$$

$$\frac{\partial}{\partial t}(\rho U_i) + \frac{\partial}{\partial x_j}(\rho U_i U_j) = -\frac{\partial P}{\partial x_i} + \frac{\partial}{\partial x_j} \left[\mu \left(\frac{\partial U_i}{\partial x_j} + \frac{\partial U_j}{\partial x_i} \right) \right] + \frac{\partial}{\partial x_j} (-\rho \overline{u_i' u_j'}) \quad (9)$$

Where ρ = density of fluid U_i = flow velocity vector and P = pressure. The Reynolds stress is expressed through the Boussinesque eddy viscosity concept as follows:

$$-\rho \overline{u_i' u_j'} = -\mu_t \left(\frac{\partial U_i}{\partial x_j} + \frac{\partial U_j}{\partial x_i} \right) + \frac{2}{3} \rho \kappa \delta_{ij} \quad (10)$$

$$\frac{\partial}{\partial t}(\rho k) + \frac{\partial}{\partial x_j}(\rho U_j k) = \frac{\partial}{\partial x_j} \left(\left(\mu + \frac{\mu_t}{\sigma_k} \right) \frac{\partial k}{\partial x_j} \right) + P_k - \rho \varepsilon \quad (11)$$

$$\frac{\partial}{\partial t}(\rho \varepsilon) + \frac{\partial}{\partial x_j}(\rho U_j \varepsilon) = \frac{\partial}{\partial x_j} \left(\left(\mu + \frac{\mu_t}{\sigma_\varepsilon} \right) \frac{\partial \varepsilon}{\partial x_j} \right) + \frac{\varepsilon}{k} (C_{1\varepsilon} P_k - C_{2\varepsilon} \rho \varepsilon) \quad (12)$$

Two partial differential equations for k and ε are used in this study to calculate Reynolds stresses:

Where μ = dynamic viscosity and μ_t = turbulent viscosity of fluid, respectively. The $P_k = \mu_t \left(\frac{\partial U_i}{\partial x_j} + \frac{\partial U_j}{\partial x_i} \right) \frac{\partial U_i}{\partial x_j}$ production rate of k . The

commonly used constant values of k - ε equations are presented in Table 1 [17].

The empirical constants are universal for a wide range of flow situations. For this reason, the k - ε model is standard in all industrial applications. Furthermore, the k - ε model shows a very stable behaviour in numerical applications.

In FLUENT, the standard wall functions are based on the proposal of Launder and Spalding [18], and have been most widely used for industrial flows. They are provided as a default option in FLUENT. The law-of-the-wall for mean velocity yields:

$$u^* = \frac{1}{k} \ln(E y^*) \quad (13)$$

Where

$$u^* \equiv \frac{u_p C_\mu^{1/4} k_p^{1/2}}{u_\tau} \quad (14)$$

$$y^* \equiv \frac{\rho C_\mu^{1/4} k_p^{1/2} y_p}{\mu} \quad (15)$$

and, k = von Karman constant (= 0.41); E = empirical constant (= 9.81); u_p = mean velocity of fluid at the center of cell adjacent to wall; k_p = turbulence kinetic energy at the center of cell adjacent to wall; y_p = distance from wall to the center of cell adjacent to wall; u_τ = shear velocity. The logarithmic law for mean velocity is known to be valid for $y^* >$ about 30 to 60. In FLUENT, the log-law is employed when $y^* >$ 11.225. When the mesh is such that $y^* <$ 11.225 at the wall-adjacent cells, FLUENT applies the laminar stress-strain relationship that can be written as:

$$u^* = y^* \quad (16)$$

TABLE 1. Constant Values of k - ε Equations.

C_μ	$C_{1\varepsilon}$	$C_{2\varepsilon}$	σ_k	σ_ε
0.09	1.44	1.92	1.00	1.30

It should be noted that, in FLUENT, the laws-of-the-wall for mean velocity are based on the wall unit, y^* , rather than y^+ ($\equiv \rho u_* y / \mu$). These quantities are approximately equal in equilibrium turbulent boundary layers.

In the present paper, a 50×548 two-dimensional staggered rectangular grid was generated with the Gambit code for analyzing the flow through the experimental flume. In order to solve Equations 7-11, boundary conditions are required at the inlet, wall, free surface and outlet. In this study, the standard wall functions and the symmetry boundary (the shear stress and all fluxes become zero) were used as for the wall and free surface boundary, respectively. A uniform velocity based on the mean velocity of the flow which measured experimentally and will be discussed later, is applied at the inlet (U_{in}). The outlet boundary condition was used to model flow exit at the flume outlet. Although no information was available for the turbulent kinetic energy at the inlet of the flume, numerical tests indicated that when the level of the turbulence intensity, based on the inlet velocity (U_{in}), was increased from 2 % to 5 % no significant change was observed in the predicted flow. Therefore, an intensity of 2 % was used in the calculation of all results shown in this work. The distribution of the dissipation rate at the inlet was estimated by introducing the hydraulic radius of the flume [18]. Finally, the SIMPLE algorithm of the FLUENT™ code was used for solving the discretized equations. As noted before the standard $k-\epsilon$ model is used as a turbulent model and the computation is continued until the simulation converged with a total relative error of less than 10^{-5} .

5. EXPERIMENTAL SET-UP AND HYDRAULIC CONDITIONS

5.1. Experimental Set-Up The experiments were conducted in a recirculating experimental flume with a width of $B = 10$ cm, length $L = 274$ cm and height of 30 cm. The bottom of the channel was covered with plastic, while the sides were manufactured from glass. An inlet tank, a contraction and turbulence damping screens condition the flow at entry to the flume. The flume terminates in an outlet tank and a reservoir. The inflow is adjusted by a control valve, while the depth of the water is varied using a rectangular weir installed in the outlet tank. The flow depth at each point of the experimental flume was measured using a graduated ruler mounted on the instrument carriage. Figure 2 presents a side view of the experimental flume and its lateral equipment.

Usually, for PIV measurements, 2D flows are illuminated with the use of a laser; in most current systems this would be a pulsed YAG laser with 15 to 150 mJ light output. The use of the laser requires extensive safety measures, e.g. locked laboratory, special training of the operators, laser-proof covers, no reflective surfaces etc. Apart from that, lasers are very costly pieces of equipment. In hydraulic modeling, the models are usually quite large compared with models in mechanical or aeronautical engineering. Many practical problems and hydraulic structures can be regarded as two-dimensional. In addition, accuracy requirements in hydraulic engineering are not as strict as they would be e.g. in aeronautical engineering and

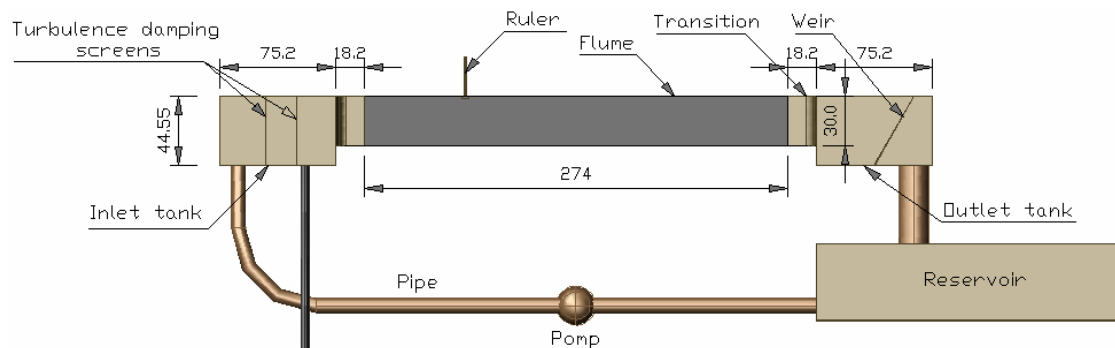
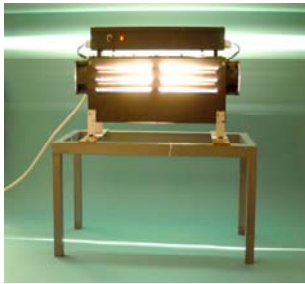


Figure 2. Experimental flume configuration.

particle velocities are much smaller. It was therefore felt that in hydraulic model testing, a system with relaxed parameters, such as wider light sheets and pulse durations of more than a few nanoseconds, could be usefully employed without any loss in accuracy of the results. In order to overcome the safety problems and the cost issues,

in this study, a white light PIV (WL PIV) system for use in hydraulic model testing was developed (Figure 3).

The light source is a white cylindrical tube (length 500 mm, diameter 10 mm) with 1000ws power mounted in a metallic box with dimensions of 100×200×600 mm. As shown in Figure 4, a slot



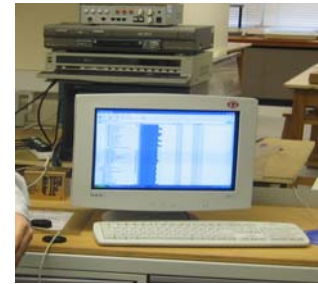
(a) White light source



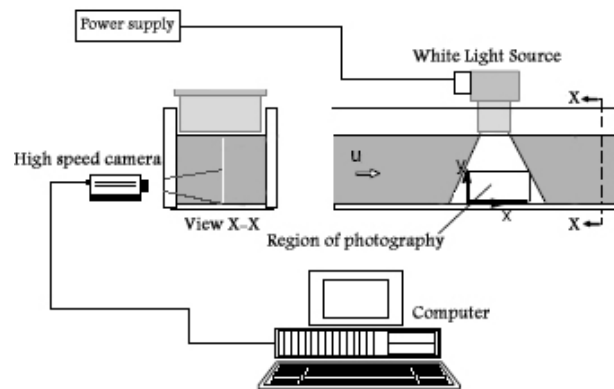
(b) Seeding particles



(c) Camera



(d) Computer



(e) Experimental arrangement for PIV

Figure 3. Experimental setup used in PIV.

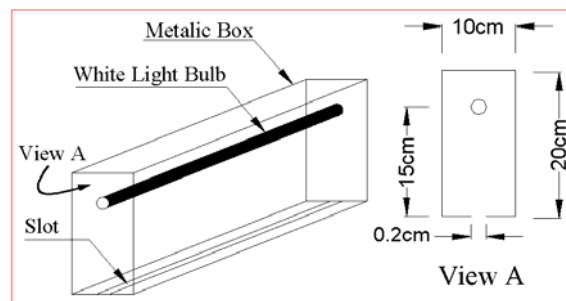


Figure 4. White light source configuration.

with 2 mm width is opened at the bottom of the box and the light tube is placed at 150 mm from the bottom. Thus, the light is scattered from the slot in a plane with diverging rate of 1:15. The bottom of the box is located at 50 mm above the water surface and adjusted so as to create a shiny plane at the center line of the flume. The thickness of light at the top of the water surface is about 2 mm wide and it is 4 mm wide at the bottom of the flume which is 200 mm below the surface. Since, the direction of seeding particles confirms that the flow is almost two dimensional in the flume, therefore the divergence created by the white light source does not influence the results.

The water was seeded with poliolite with a diameter 0.3-0.5 mm and density of 1.03 gr/cm³ as tracer particles. The field-of-view was imaged with a high speed camera (Photron Fastcam PC1 1024) with a time interval of 1/50s and resolution of 1024×1024 pixels. The camera was fitted with a lens (focal-length range of 50 to 400 mm) and the object distance was adjusted to obtain a field-of-view of 120 mm in X-direction and 90 mm in Y-direction. Commercial software (MatPIV) [19] was used to perform the image analysis using a cross-correlation technique. Each captured frame was separated into odd and even fields to obtain the temporal information. The white levels of the pixels in the correlation area of the first and second fields were cross-correlated within the searching area. Using an interrogation area of 64×64 pixels, the correlation peak was evaluated in a search area formed by a circle of radius equal to 15 pixels. Therefore the velocity vectors are obtained based on pixel resolution.

5.2. Experimental Conditions To investigate the accuracy of WL PIV technique in different flow conditions, experiments were done at three

different values of flow rates. The hydraulic conditions are summarized in Table 2; here, Q is the flow rate, h the flow depth, $U_m = Q/(hB)$ the mean velocity, R the hydraulic radius, $Re = 4U_m R/\nu$ the Reynolds number ($\nu = 1 \times 10^{-6} \text{m}^2/\text{s}$ kinematic viscosity of water at 20°C), $F = U_m / \sqrt{gh}$ the Froude number, $U_{\tau_{log}}$ and $U_{\tau_{uv}}$ the shear velocities obtained from various methods and $Re_{\tau} = 4U_{\tau_{uv}} R/\nu$ the Reynolds shear stress.

As the shear velocity U_{τ} which is used in the analysis of the velocity profiles, is the quantity most likely to be subjected to errors from both experimental methods and data analysis, in the present work its evaluation was made using two methods as follows:

- An alternative method frequently applied to determine the shear velocity $U_{\tau_{log}}$ is based on the best-fit of the measured mean velocity distribution to the logarithmic law, i.e. Equation 5.
- The shear velocity $U_{\tau_{uv}}$ can be evaluated from the measured Reynolds stress of fluid. For a two-dimensional open channel flow, the vertical distribution of Reynolds stress, $-\overline{u'v'}$, is given by [13]:

$$\frac{-\overline{u'v'}}{U_{\tau}^2} = \left(1 - \frac{y}{\delta}\right) \quad (17)$$

According to this method, the shear velocity $U_{\tau_{uv}}$ can be determined by an extrapolation of the measured Reynolds stress $-\overline{u'v'}$ to $y = 0$.

The values of both $U_{\tau_{log}}$ and $U_{\tau_{uv}}$ for the three experiments obtained based on the two

TABLE 2. Hydraulic Conditions.

Experiment No.	Q [l/s]	h [cm]	U_m [cm/s]	R	Re	F	$U_{\tau_{log}}$	$U_{\tau_{uv}}$	Re_{τ}
1	2.0	0.21	0.0955	15427	20055	0.066	0.0066	0.0063	1018
2	3.02	0.215	0.136	22068	29240	0.093	0.0081	0.0079	1281
3	4.27	0.22	0.194	31615	42680	0.132	0.011	0.0107	1743

mentioned methods are presented in Table 2. It can be seen that a good and similar estimate of the shear velocity using the two methods. In this study, to compare the analytical data and the experimental observation, the values of $U_{\tau_{uv}}$ were used.

6. RESULTS AND DISCUSSIONS

The 500 instantaneous velocity fields were sampled to obtain the mean velocities and Reynolds stresses. The image couples were analyzed using the MatPIV analysis software package employing 64×64 pixels with 50 % overlapping. The analysis produced about 200 vectors per map, filtered by using standard median and global outlier filters. About 5 % of the erroneous vectors were removed during the post-processing analysis. The resulting velocity vector fields were then brought into the global co-ordinate system.

Figure 5 shows the time-averaged displacement vectors of the seeding particles were generated using PIV cross-correlation analysis in a viewing window $120 \text{ mm} \times 90 \text{ mm}$. The viewing window covers the bed of the flume with a height of 0.09 m extended from $x = 1.40 \text{ m}$ to $x = 1.52 \text{ m}$ of the flume entrance. Averaging is done over 500 WL PIV images. By dividing the displacement vectors to the time interval between two images, velocity field for each experimental case was obtained.

In order to evaluate the WL PIV measurements, a test section A-A (see Figure 5) located 1.42 m downstream of the flume entrance was selected. Figure 6 shows the calculated time series of the two velocity components using all 500 images at 10 second at a point with $y = 0.01 \text{ m}$ on the test section. Averaging the whole data set obtained from analysis of all 500 images along the test section in the three experiments were done. In Figure 7, the mean velocity profile of all three experiments at section A-A are shown. According to the mean velocity profiles, boundary layer thickness (δ) in experiments No.1 through No.3 is measured 49, 46 and 41 mm, respectively.

The WLPIV measurements should be validated by comparison of the experimental values with empirical results, numerical simulations or with

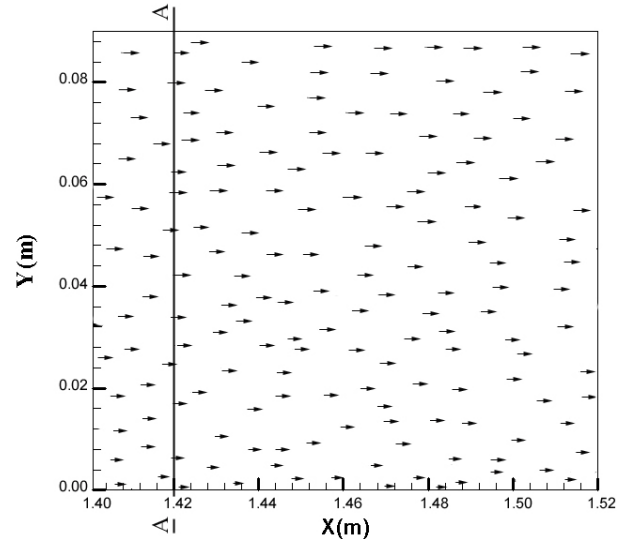


Figure 5. Visualization of velocity field obtained by PIV in experiment No. 1.

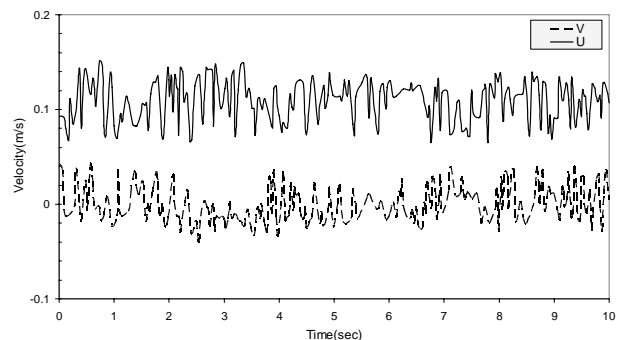


Figure 6. Time series of the two velocity components for experiment No. 1 at point $y = 0.01 \text{ m}$ on test section A-A.

other measurements. Figure 8 shows the distributions of Reynolds stress for all cases in the present study. Based on the values of $U_{\tau_{uv}}$ and δ

and substituting both of them in Equation 17, WL PIV measurements are compared with analytical results in Figure 8. From the figure, PIV data are in good agreement with the theoretical results. Figure 9 compares the stream wise mean velocity profile estimated from the WL PIV measurements to the empirical results. In this figure, the velocity profiles of $U^+ = U/U_\tau$ versus $y^+ = yU_\tau/\nu$ are normalized by the values of $U_{\tau_{uv}}$. It should be

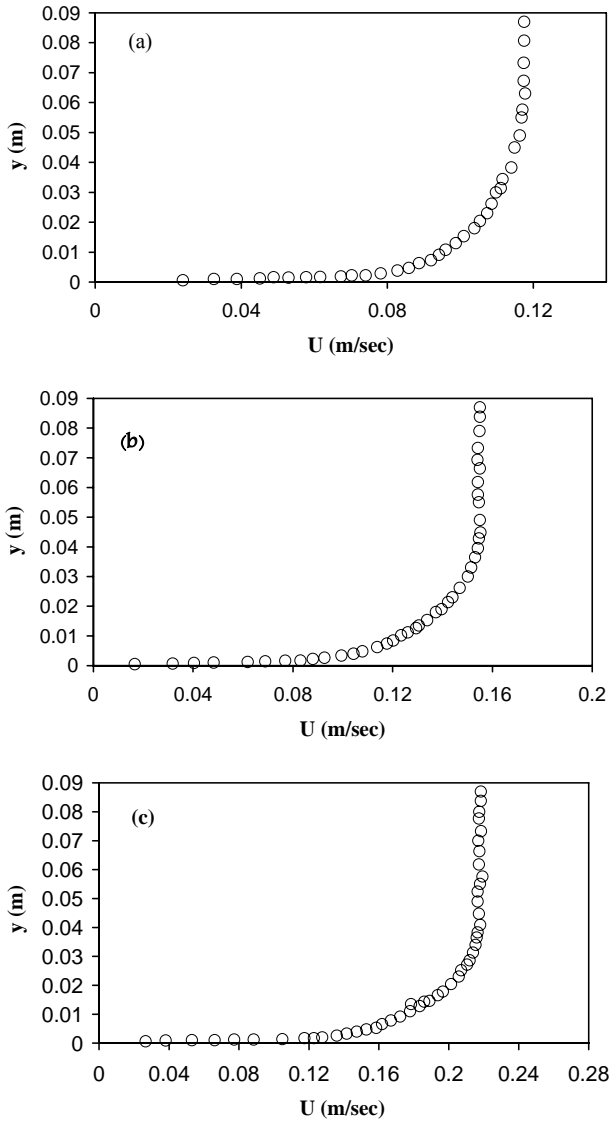


Figure 7. Measured mean velocity profile at test section A-A in experiment No. (a) 1, (b) 2 and (c) 3.

noted that WL PIV data in Figure 8 coincide well with the theoretical curves.

In this study, the flow through the experimental flume was modeled computationally using the Reynolds averaged 2-D Navier-Stokes equations and the $k-\epsilon$ turbulence model of FLUENTTM. The velocity profile obtained by PIV in section A-A are compared with the numerical results (Figure 10). It was found that for experiment No.1 through No.3, the WL PIV measurements have 0.5, 0.7 and 1.5 percent deviation, respectively, from the

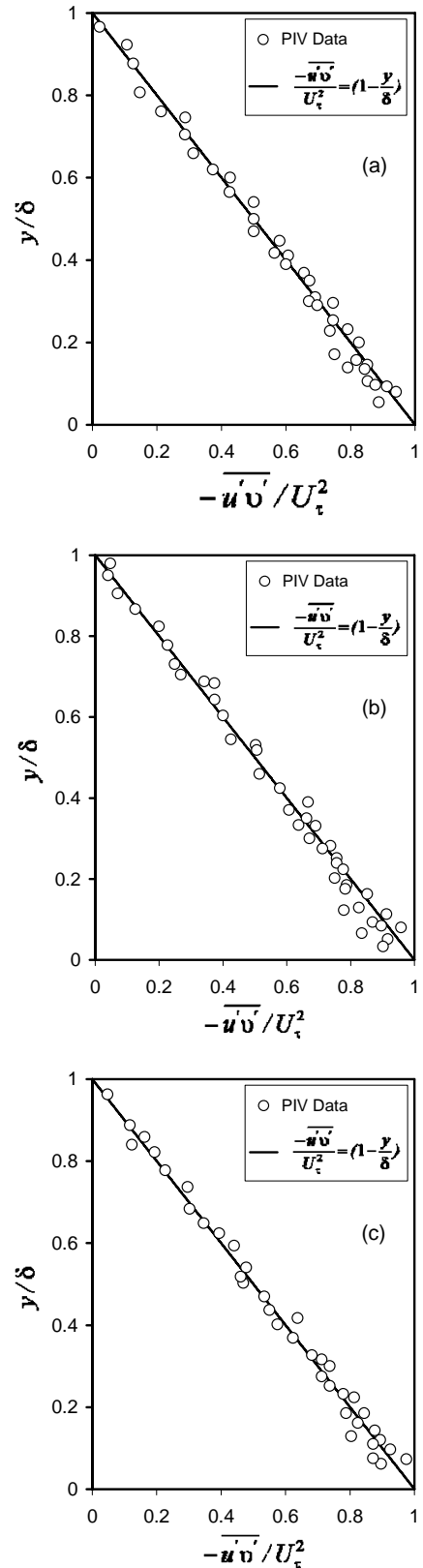


Figure 8. Measured Reynolds stress distribution in boundary layer of section A-A in experiment No. (a) 1, (b) 2 and (c) 3.

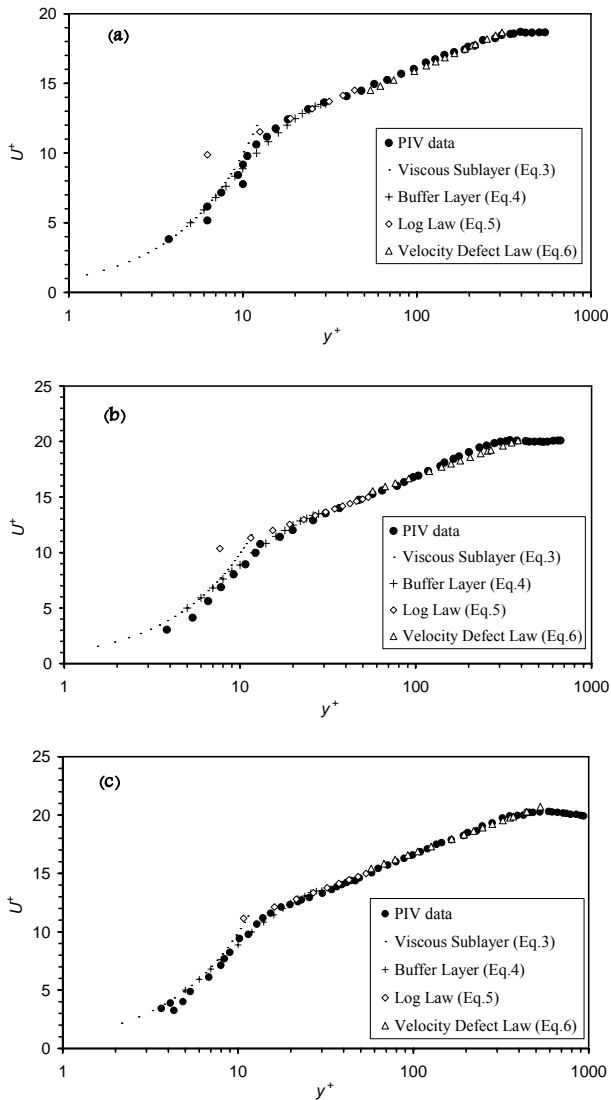


Figure 9. Comparison of mean velocity profile of WL PIV measurements and the empirical results in experiment No. (a) 1, (b) 2 and (c) 3.

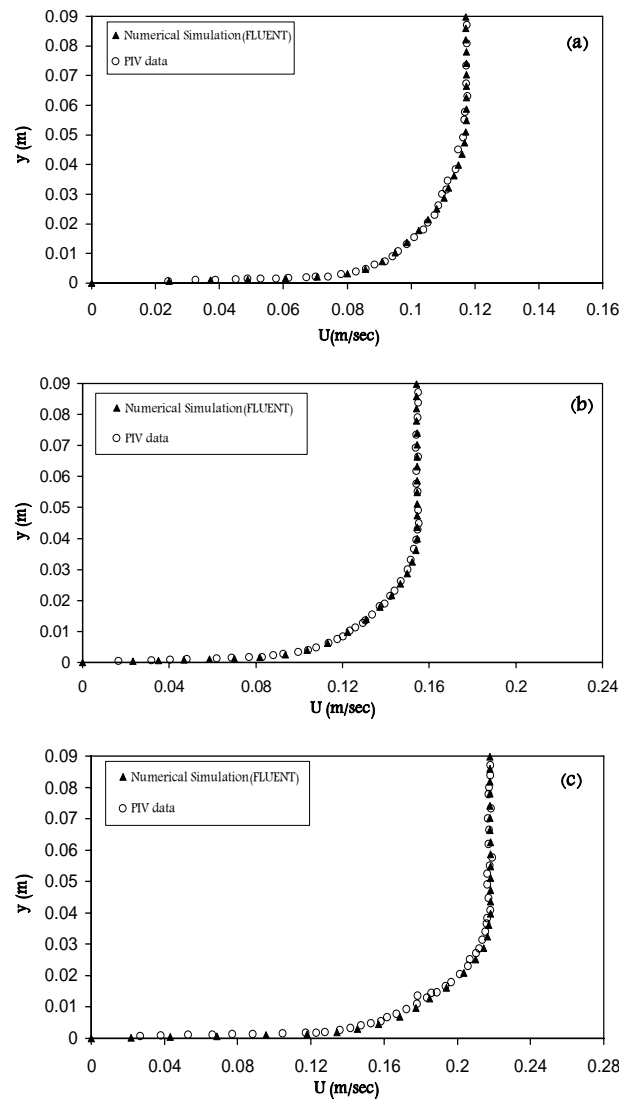


Figure 10. Mean velocity profile at A-A section obtained with WL PIV and CFD in experiment No. (a) 1, (b) 2 and (c) 3.

computational velocities. This clarifies the higher accuracy of the WL PIV used in this present study in analyzing the open channel flow.

7. CONCLUSION

In this work, a comparison of both WL PIV measurements and empirical data and CFD

simulation was made. The objective of the work was to assess the white light sheet PIV as a cost-effective and safe alternative for laser systems whilst keeping the accuracy limits required for hydraulic model tests. The accuracy requirements for experimental work in hydrodynamics are usually less stringent than in aeronautical and mechanical engineering. Models in hydraulic engineering are larger, so that measurement volumes and light sheets can also be larger and wider. In addition, many hydraulic engineering

laboratories consist of open spaces, so that the safety precautions required for laser work can be very difficult to implement. A white light source for PIV applications results in significantly easier experimental conditions as well as substantially reduced costs. It should be noted that the price of this system is very low when compared with a laser PIV model (almost 1:300). The development of a white light source for PIV applications means that experiments can be conducted with a standard PIV system in virtually any location.

In this study, based on WL PIV measurements, the mean velocity profile of each experiment was validated by comparing them to the results which were obtained through empirical models of the mean velocity distribution in the boundary layer. Excellent agreement between the experimental and empirical results was observed. The results also showed that the WL PIV measured values of Reynolds stress were in good agreement with the theoretical formula in the boundary layer. For further investigation, the whole flow field in the experimental flume was modeled computationally using the two-dimensional Reynolds averaged Navier-Stokes equations and the $k-\epsilon$ turbulence model of FLUENT™ code. The comparison of WL PIV with CFD simulation velocities indicated that in a range of velocity between 0.095 to 0.194 m/s, the general error of the PIV measurement was an average of about 0.5 to 1.5 %. It provides further evidence that WL PIV can be applied successfully in open channel flow analysis.

8. ACKNOWLEDGMENTS

The first author acknowledges the financial support given by the Ministry of Education of the Islamic Republic of Iran and all the support offered by the Engineering Department of the University of Warwick, U.K. The first author is also particularly indebted to Graham Canham who assisted with the photography.

9. REFERENCES

1. Lehr, A. and Bölcs, A., "Application of a Particle Image Velocimetry (PIV) System to the Periodic

- Unsteady Flow Around an Isolated Compressor Blade", 15th Bi-annual Symposium on Measurement Techniques in Transonic and Supersonic Flow in Cascades and Turbomachines University of Florence, (2000), 1-10.
2. Meinhart, C. D., Wereley, S. T. and Santiago, J. G., "A PIV Algorithm for Estimating Time-Averaged Velocity Fields", *Journal of Fluids Engineering*, Vol. 122, (2000), 285-289.
3. Adrian, R. J., "Particle-Imaging Techniques for Experimental Fluid Mechanics", *Annual. Rev. Fluid Mech.*, No. 23, (1991), 261-304.
4. Liu, Z.-C., Landreth, C. C., Adrian, R. J. and Hanratty, T. J., "High Resolution Measurement of Turbulent Structure in a Channel with Particle Image Velocimetry", *Experiments in Fluids*, Vol. 10, (1991), 301-312.
5. Willert, C., Stasicki, B., Raffel, M. and Kompenhans, J., "A Digital Video Camera for Application of Particle Image Velocimetry in High-Speed Flows", *SPIE Proceedings*, Article, No. 2546-19, (1995), 32-39.
6. Okamoto, K. and Oki, M., "Particle Imaging Velocimetry Standard Images-Transient Three-Dimensional Images", *International Conference on Advanced Optical Diagnostics in Fluids, Solids and Combustion*, Tokyo, Japan, (2004), 1-5.
7. Hassan, Y. A., "Multiphase Bubbly Flow Visualization Using Particle Image Velocimetry", *Annals of the New York Academy of Sciences*, Vol. 972, (2002), 223-228.
8. Bryanston-Cross, P. J. and Epstein, A. H., "The application of sub-micron particle visualization for PIV (Particle Image Velocimetry) at transonic and supersonic speeds", *Progress in Aerospace Science*, Vol. 27, (1990), 237-265.
9. Towers, C., Bryanston-Cross, P. J. and Judge, T. R., "The application of PIV to large scale transonic wind tunnels", *Laser and Optics Technology*, Vol. 23, (1991), 289-296.
10. Bryanston-Cross, P. J., Towers, D., Towers, C. and Judge, T. R., "The Application of PIV in a short duration transonic annular turbine cascade", *Journal of Turbomachinery*, Vol. 114, No. 3, (1992), 504-510.
11. Dantec Dynamics, "Measurement Principles of PIV", <http://www.dantecdynamics.com/piv/princip/>, (2006).
12. Schlichting, H., "Boundary layer theory", McGraw-Hill, New York, (1979).
13. Nezu, I. and Nakagawa, H., "Turbulence in open-channel flows", IAHR-Monograph, Balkema, Rotterdam, The Netherlands, (1993).
14. Nezu, I. and Rodi, W., "Open-channel measurements with a laser Doppler anemometer", *J. Hydraul. Eng.*, Vol. 112, No. 5, (1986), 335-355.
15. Van Driest, E. R., "On turbulent flow near a wall", *J. Aeron. Sci.*, Vol. 23, (1956), 1007-1011.
16. Launder, B. E. and Spalding, D. B., "Mathematical models of turbulence", New York: Academic Press, (1972).
17. Rodi, W., "Turbulence models and their application hydraulics", IAHR-Monograph, 3rd edition Delft, Netherlands, (1993).

18. Fluent, Inc., "FLUENT User's Guide", Fluent, New Hampshire, (1993).
19. GNU/GPL, MATPIV, "Software home page", <http://www.math.uio.no/~jks/matpiv/>, (2006).